

# Infrared properties of the SDSS-maxBCG galaxy clusters

M. Roncarelli<sup>1</sup>, E. Pointecouteau<sup>1</sup>, M. Giard<sup>1</sup>, L. Montier<sup>1</sup> and R. Pello<sup>2</sup>

<sup>1</sup> Centre d'Etude Spatiale des Rayonnements, CNRS/Université de Toulouse, 9 avenue du Colonel Roche, BP44346, 31028 Toulouse Cedex 04, France.

e-mail: mauro.roncarelli@cesr.fr

<sup>2</sup> Laboratoire d'Astrophysique de Toulouse-Tarbes, Université de Toulouse, CNRS, 14 Av. Edouard Belin, 31400 Toulouse, France.

Accepted ??? Received ???; in original ???

## ABSTRACT

**Context.** The physics of galaxy clusters has proven to be influenced by several processes connected with their galactic component which pollutes the intracluster medium (ICM) with metals, stars and dust. However, it is not clear whether the presence of diffuse dust can play a role in clusters physics since a characterisation of the infrared (IR) properties of galaxy clusters is very challenging and yet to be completely achieved.

**Aims.** In our study we focus on the recent work of Giard et al. (2008) who performed a stacking analysis of the IRAS data in the direction of several thousands of galaxy clusters, providing a statistical characterisation of their IR luminosity and redshift evolution. We model the IR properties of the galactic population of the SDSS-maxBCG clusters ( $0.1 < z < 0.3$ ) in order to check if it accounts for the entire observed signal and to constrain the possible presence of other components, like dust in the ICM.

**Methods.** Starting from the optical properties of the galaxies of the SDSS-maxBCG clusters, we estimate their emission in the 60 and 100  $\mu\text{m}$  IRAS bands making use of modeled spectral energy distributions of different spectral types (E/S0, Sa, Sb, Sc and starburst). We also consider the evolution of the galactic population/luminosity with redshift.

**Results.** The total galactic emission, which is dominated by the contribution of star-forming late-type galaxies, is consistent with the observed signal. In fact, our galactic emission model slightly overestimates the observed fluxes, with the excess being concentrated in low-redshift clusters ( $z \lesssim 0.17$ ).

**Conclusions.** Our results indicate that, if present, the IR emission from intracluster dust must be very small compared to the one associated to the galaxy members. This translates into an upper limit on the dust-to-gas mass ratio in the ICM of  $Z_d \lesssim 5 \times 10^{-5}$ . The excess in luminosity obtained at low redshift constitutes an indication that the cluster environment is driving a process of star-formation quenching in its galaxy members.

**Key words.** cosmology: large scale structure of Universe – galaxies: clusters: general – intergalactic medium – infrared: galaxies

## 1. Introduction

Clusters of galaxies form in correspondence of the peaks of the primordial matter density field as a result of the gravitational collapse of both dark matter and baryons. In the framework of the standard  $\Lambda\text{CDM}$  cosmological model and the hierarchical clustering of the large scale structure formation they constitute both the most recent and the largest virialised objects of the Universe.

Nowadays, it is clear that gravitation is not the only process that influences the physics of the intracluster medium (ICM, hereafter). The electrons of the ionized plasma emit via free-free interaction with the protons, making clusters bright X-ray sources and allowing the gas to cool efficiently, particularly in the central regions. During the last decade, the observations of the *XMM-Newton* and *Chandra* X-ray satellites highlighted the presence of several interaction mechanisms between the galactic component and the ICM, showing that the evolution of the two is intimately tied. For instance, the accretion of cold gas onto the brightest cluster galaxies (BCGs) at the cluster center is strongly suspected to fuel the super-massive blackholes they host. This process is able to trigger star-formation within the BCGs (O'Dea et al. 2008; Pipino et al. 2009) and power episodic violent outbursts of their central active galactic nuclei (AGNs), whose energy injection into the ICM prevents the overcooling of the gas (Fabian et al. 2006; McNamara & Nulsen 2007).

AGNs feedback and other non-gravitational processes, such as supernovae (SNe) powered galactic winds (Kapferer et al. 2006; Sijacki & Springel 2006; Schindler & Diaferio 2008), preheating of the ICM (see e.g. Fang & Haiman 2008), together with gravitational ones (i.e. galaxy-galaxy interactions, ram-pressure stripping, galaxy mergers) induce energy and matter exchanges between the galactic medium and the ICM. To date these complex physical processes and their impact on the statistical cluster properties, thus on our understanding of structure formation (Voit 2005) and use of the cluster population in cosmological studies (Mantz et al. 2008; Vikhlinin et al. 2009; Mantz et al. 2009), are under scrutinous observational and theoretical investigations (see, e.g., Arnaud 2005; Borgani 2008a, and references therein).

The presence of heavy elements in the ICM is the most direct evidence and consequence of the ejection of galactic material. Within clusters their abundance has been widely measured making use of X-ray observations (see the reviews by Sarazin 1988; Arnaud 2005; Werner et al. 2008) with a typical abundance of  $0.3 Z_{\odot}$ . Stars and SNe constitute the most efficient way to produce and disperse metals. Heavy elements in the ICM originate from different processes: early enrichment (Aguirre & Schaye 2007), continuous injection from galaxy members and in situ production by intra-cluster stars (sources of the intra-cluster light, see Arnaboldi 2004; Krick & Bernstein

2007; Murante et al. 2007; Conroy et al. 2007; Dolag et al. 2009). The aforementioned processes do not discriminate between the natures of the ejected galactic material, therefore these enrichments are unambiguously linked also to the ejection of neutral gas and dust in the ICM.

Observations indicate that in galactic environments dust is a minor component, with dust-to-gas ratio  $M_{\text{dust}}/M_{\text{gas}} \approx 0.01$  (Mathis et al. 1977) and it could be as low as  $M_{\text{dust}}/M_{\text{gas}} = 10^{-5} - 10^{-4}$  in the ICM (Popescu et al. 2000; Aguirre et al. 2001). Nonetheless, dust particles have lifetimes long enough to be heated by collisions with the hot electrons and re-emit at the infrared (IR) wavelengths. In this way they can constitute an additional cooling agent of the gas (Montier & Giard 2004) which might play an important role in ICM physics, as seen with the implementation of dust cooling in hydrodynamical simulations (da Silva et al. 2009).

However obtaining observational constraints on the possible IR signal coming from intracluster dust is a very challenging issue, since the average sky fluctuations caused by background galaxies and galactic cirrus clouds are comparable or even higher than the overall flux coming from a single cluster, which is anyway expected to be dominated by the dust emission from star-forming galaxies. In fact, nowadays the only claimed (and still controversial) detection of this IR emission comes from the studies on the Coma cluster of Stickel et al. (1998, 2002), who measured a diffuse dust mass of  $M_{\text{dust}} \approx 10^7 M_{\odot}$ , while other attempts resulted in non detections (see, e.g., Bai et al. 2007).

If studies on single objects appear very problematic, the low signal-to-noise problem can be overcome by adopting a statistical approach, taking advantage of the high number of clusters detected mainly with optical surveys (see Biviano 2008, for a review). This concept was first used at IR wavelengths by Montier & Giard (2005) who performed a stacking analysis of the *Infra Red Astronomical Satellite* (IRAS) survey in the direction of more than 11 000 known galaxy clusters and groups and obtained a statistical detection of the overall clusters signal at 12, 25, 60 and 100  $\mu\text{m}$ . Starting from this result, Giard et al. (2008) characterised the IR luminosity evolution of the stacked sample, analysing also its correlation with their X-ray luminosities. These works constitute a first important result on the global IR properties of galaxy clusters. However, since the clusters IR emission could be dominated by star-forming galaxies, it becomes crucial to disentangle the galactic signal from a possible diffuse component in order to quantify its implications on cluster physics. On the other side, understanding the IR properties of the cluster galaxies could provide hints on the environmental effects over their star-formation, which are nowadays objects of studies at different wavelengths, from the radio to the ultraviolet (UV, see Boselli & Gavazzi 2006a, for a review).

In this work we attempt to reconstruct the observed stacked IR emission measured in the direction of galaxy clusters in the IRAS whole sky survey. We model in details the contribution of cluster galaxies to the total IR emission in order to understand whether this contribution is sufficient to explain the fluxes and luminosities derived by Montier & Giard (2005) and Giard et al. (2008) or if, on the contrary, there is an indication of a non-galactic component, possibly associated to intracluster dust. Since for our modelisation we make use of the known spectral properties of galaxies as observed mainly in the field, the comparison between our results and observed data can be useful also to highlight possible differences between cluster and field galaxies.

This paper is organised as follows. In the next Section we briefly present the statistical detection of the clusters IR emis-

sion of Montier & Giard (2005) and Giard et al. (2008) and we focus in particular on the subsample of the SDSS-maxBCG catalogue. In Section 3 we describe the details of our modelisation for the IR luminosity of cluster galaxies and discuss the possible presence of other galactic components in Section 4. In Section 5 we apply our model to estimate the IRAS fluxes, then our results are discussed in Section 6. Finally, we present our conclusions in Section 7.

Throughout this paper we assume a flat  $\Lambda$ CDM cosmological model with  $(\Omega_{\Lambda}, \Omega_{\text{m}}, h) = (0.7, 0.3, 0.7)$ .

## 2. The statistical IR emission of clusters

Working on a list of 11 507 groups and clusters selected from 14 publicly available catalogues,<sup>1</sup> Montier & Giard (2005) performed a clear statistical detection of the IR flux in the direction of galaxy clusters by stacking their corresponding fields (within 10' from the cluster center) in the IRAS all sky survey. After dealing carefully with the point sources contamination, foreground/background subtraction and other various systematic effects, they measured stacked fluxes at 60 and 100  $\mu\text{m}$  with signal-to-noise ratio of 57 and 43 respectively. Over the four IRAS wavelengths this emission proves to be consistent with the spectral signature of galactic IR emission.

More recently, on the basis of Montier & Giard (2005) results, Giard et al. (2008) performed a statistical analysis in redshift, presenting for the first time the evolution of the IR luminosity of galaxy clusters. In addition to Montier & Giard (2005) original list of 11 507 clusters, Giard et al. (2008) backed-up their analysis on two *standalone* catalogues – i.e. the “*Northern Sky Optical Cluster Survey*” (NSC, Gal et al. 2003), and the SDSS-maxBCG catalogue (Koester et al. 2007) – for which a richness information was available. They extended their IRAS stacking analysis to the *Rosat All Sky Survey* (RASS, Voges 1992) in order to compare the evolution in redshifts of the IR and X-ray luminosity. They showed that the stacked IR luminosities are on average 20 times higher than the X-ray luminosities. They also found that the IR luminosity is evolving rapidly as  $(1+z)^5$  in the  $0.1 < z < 1$  interval. Giard et al. (2008) also made use of the richness information (i.e. correlated to the halo occupation number), contained in the SDSS-maxBCG and NSC catalogues, to constrain the dependence of the IR luminosities with cluster richness. They derived a correlation following  $L_{\text{IR}} \propto (N_{\text{gal}}^{R200})^{0.8 \pm 0.2}$ .

In order to understand the aforementioned results at 60 and 100  $\mu\text{m}$ , in this work we focus on the modelisation of the IR luminosity and fluxes of galaxy clusters. The IR spectrum of galaxies, which is dominated by dust emission (Lagache et al. 2005; Soifer et al. 2008), is expected to make a major contribution to the IR emission detected in the direction of clusters (Giard et al. 2008). Therefore, a careful modeling of the IR emission of member galaxies is needed in order to understand the global properties of clusters in the IR, and in particular to disentangle between the relative contribution of galaxies and intracluster dust. Given the inhomogeneity of the main dataset used by Montier & Giard (2005) and Giard et al. (2008) (i.e. the 11 507 groups and clusters) in terms of cluster size and detection method, it becomes

<sup>1</sup> The list was build making use of the SIMBAD database, operated at CDS, Strasbourg, France (<http://simbad.u-strasbg.fr/simbad/>) and NASA/IPAC Extragalactic Database (NED), operated by the JPL/Caltech (<http://nedwww.ipac.caltech.edu>), among which the ABELL catalogue (Abell et al. 1989) and the “*Northern Sky Optical Cluster Survey*” (NSC, Gal et al. 2003).

very difficult to define a global selection function of such sample, that would be necessary in order to have a suitable starting base for our work. In order to overcome these difficulties we decided to base our modelisation on a restricted and well defined cluster sample by considering a single catalogue. For the purpose of our calculations we chose the SDSS-maxBCG catalogue.

### 2.1. The SDSS-maxBCG catalogue

Since we want to reconstruct the total IR luminosity and flux due to cluster galaxies, we require an information on the halo occupation number (i.e. the number of galaxies within the cluster potential well). In this view the SDSS-maxBCG catalogue (Koester et al. 2007) is the most fitted to our needs. Indeed, since the SDSS-maxBCG catalogue is created by identifying overdensities in the galaxy distribution, it contains information about the richness of the cluster itself that we can use directly without having to deal with the uncertainties connected with the  $N - M$  and  $L_X - M$  relations, that would be necessary, for instance, in case of X-ray selected clusters. Moreover, the number of objects contained in the SDSS-maxBCG catalogue is the highest among all the others (i.e. 13 807 groups and clusters), thus providing a good statistics which is needed to assess the robustness of our results. Finally, Koester et al. (2007) provide also the total luminosity in the  $r$  and  $i$ -band of the identified cluster members which also have a well defined spectral type (E/S0 galaxies). We will make use of this information to obtain an estimate of their flux in the IRAS bands (see Sect. 3).

The SDSS-maxBCG catalogue has been obtained by analysing the clustering properties of more than 500 000 SDSS galaxies in an area of  $\sim 7\,500\,\text{deg}^2$  in the redshift range  $0.1 < z < 0.3$ . For each cluster the catalogue contains a photometric redshift and an indication of the cluster richness,  $N_{\text{gal}}^{R200}$ . This quantity corresponds to the number of early-type galaxy members at a distance lower than  $R_{200}$  from the central BCG. The adopted definition of  $R_{200}$  is the radius at which the deprojected galactic density is  $200\,\Omega_m^{-1}$  times the average galactic density on the large scale: in the approximation of galaxies following the matter distribution, this is equivalent to the usual cosmological definition of  $R_{200}$  as the radius enclosing a density 200 times larger than the critical density of the Universe (see the discussion in Hansen et al. 2005, for details).

It is important to note that  $N_{\text{gal}}^{R200}$  does *not* represent the total cluster richness because it does not include spiral galaxies: in fact, the cluster members candidates have been selected for having colors matching the E/S0 ridgeline (Bower et al. 1992) and  $M_r < -16$ . We will explain in the detail our definition of the cluster richness in Section 3.2.

The SDSS-maxBCG catalogue includes 13 823 groups and clusters with  $N_{\text{gal}}^{R200} \geq 10$  and it is widely dominated by the presence of groups and small clusters ( $N_{\text{gal}}^{R200} \approx 10 - 15$ ). As a reference, when computing their corresponding  $M_{200}$  with the relation of Rykoff et al. (2008), the median of the mass distribution is  $4.5 \times 10^{13} h^{-1} M_\odot$ . In this work, we adopted the trimming done by Giard et al. (2008) on the SDSS-maxBCG catalogue of objects located in regions of the sky not covered by the IRAS data, with noisy images, or whose fields contain strong IR sources. This selection process ended up in a sample of 7 476 clusters, corresponding to a total of 121 318 E/S0 galaxy members, that will be the object of our analysis.

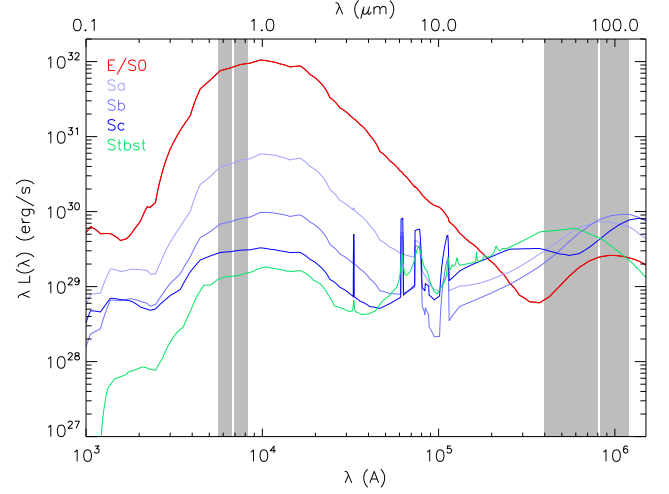


**Fig. 1.** SEDs as a function of wavelength for the 5 GRASIL (Silva et al. 1998) templates used in this work. The red line shows our reference model for E/S0 galaxies, the three blue lines represent normal spiral galaxies Sa, Sb, Sc (light blue, average, dark blue, respectively) and the green line represents our starburst galaxy model, corresponding to M82. All of the templates have been arbitrarily normalized to the same integrated luminosity of  $10^{30}$  erg/s in the band 8-1000  $\mu\text{m}$  (i.e. IR luminosity,  $L_{\text{IR}}$ ). The four shaded regions identify the optical  $r$  and  $i$ -band and the two IRAS bands of 60  $\mu\text{m}$  and 100  $\mu\text{m}$ , from left to right.

### 3. Modeling galaxy luminosities

The main source of the IR radiation of galaxy clusters is expected to be the thermal emission due to the dust reprocessing the UV photons emitted by stars inside cluster galaxies. Since we are basing our work on galaxies observed in the optical band, we need to construct a valid model that is able to connect their galactic  $r$  band emission to the corresponding dust emission in the IR. In particular, we will focus on the 60  $\mu\text{m}$  and 100  $\mu\text{m}$  IRAS bands fluxes, in order to compare our results with the most relevant measurements of Giard et al. (2008). The characteristics of the galactic IR emission depend on the amount of dust present in the galaxies and are strictly connected with their star-formation rate (SFR) and, therefore, their spectral type.

Spectral energy distribution (SED) templates obtained with the spectral synthesis code GRASIL (Silva et al. 1998) were used in order to represent the typical emission of galaxies in the local universe. GRASIL SEDs extend from UV to radio wavelengths, including dust reprocessing and nebular line emission. We used four templates for normal galaxies, with Salpeter's initial mass function and age 13 Gyr, namely an elliptical galaxy and three different spiral galaxies (Sa, Sb and Sc). We also included the GRASIL model fit to multi-wavelength observations of M82 as a semi-empirical template to represent the typical SED of local starburst galaxies (Silva et al. 1998). For spiral galaxies, the SEDs correspond to a weighted average over the different lines of sight, from face-on to edge-on, in order to statistically account for the mean spatial orientations of cluster galaxies. The five templates are displayed in Fig. 1.

The SED models described above were used to derive the expected IR luminosities from observed fluxes and corresponding luminosities in the  $r$  band. For a given template, the luminosity in the  $r$  band is given by

$$L_r = \int L(\lambda) T_r(\lambda) d\lambda, \quad (1)$$

**Table 1.** Reference spectral types and galactic population models used in this work.

Spectral type	Population (%)			$u-r$	$R_{\text{IR},r}$
	no ev.	ref.	cons.		
<i>-Early-type</i>					
BCG	4.3	4.0	4.2	—	0.12
E/S0	65.4	61.5	63.3	—	0.12
(Tot. early-type)	(69.7)	(65.5)	(67.5)		
<i>-Late-type</i>					
Sa	4.4	5.1	6.5	>2.2	2.36
Sb	9.6	10.7	11.7	1.8–2.2	13.82
Sc	15.8	18.2	14.1	1.0–1.8	33.80
Starburst	0.5	0.5	0.2	<1.0	73.16
(Tot. late-type)	(30.3)	(34.5)	(32.5)		

The fraction (in percentile) of each type of galaxies in the three population models is shown: without redshift evolution, in our reference model and for the conservative scenario (second to fourth column, respectively). The fifth column shows the corresponding intrinsic  $u-r$  color intervals used for the modelisation of the spirals (early-type galaxies are taken directly from the SDSS-maxBCG catalogue). The last column shows the values of the ratio  $L_{\text{IR}}/L_r$  for each template.

where  $L(\lambda)$  is the luminosity per unit wavelength and  $T_r(\lambda)$  is the SDSS  $r$  filter transmission. For the purpose of this work, we define the IR luminosity following Le Floc'h et al. (2005):

$$L_{\text{IR}} = \int_{8\mu\text{m}}^{1000\mu\text{m}} L(\lambda) d\lambda. \quad (2)$$

Therefore, for each template SED, the scaling ratio can be defined as follows

$$R_{\text{IR},r} \equiv \frac{L_{\text{IR}}}{L_r}. \quad (3)$$

Table 1 summarizes the  $R_{\text{IR},r}$  values for the different templates used in this paper. For a given  $L_r$ , the corresponding  $L_{\text{IR}}$  can be different by almost three orders of magnitude depending on the spectral type of the galaxy. The modelisation of the luminosity of early-type and late-type galaxy populations is explained in the details in the next sections.

### 3.1. Early-type galaxies

Early-type galaxies are characterized by an old stellar population and a star-formation history which is essentially compatible with passive evolution: for this reason they are not expected to dominate the emission in the IRAS bands. In fact, for a fixed  $L_{\text{IR}}$ , the amount of energy emitted at wavelengths  $\lambda \gtrsim 40 \mu\text{m}$  is one order of magnitude lower with respect to normal spirals (see Fig. 1). However, it is known that in dense environments elliptical galaxies largely dominate the galactic population, being about 4 times more frequent than spirals (see, e.g., Dressler 1980; Dressler et al. 1997). Moreover red galaxies are usually more massive and more luminous in the  $r$  band than blue ones. For these reasons their total contribution on the clusters IR signal may be non-negligible.

As mentioned in Section 2.1, Koester et al. (2007) identified the number  $N_{\text{gal}}^{R200}$  of E/S0 galaxies ( $M_r < -16$ ) inside  $R_{200}$  of each of the 7 476 clusters of our sample. For each cluster, the authors provide the luminosity,  $k$ -corrected at  $z=0.25$ , in the  $r$  band, of the BCG and of the other E/S0 members as a whole. We corrected these luminosities into rest-frame luminosities by using

the LRG template of KCORRECT (Blanton & Roweis 2007): we refer to  $L_r^{\text{BCG}}$  and  $L_r^{\text{memb}}$  for the luminosity of the BCG and of the cluster as a whole, respectively, after this correction. Given the uniform properties of early-type galaxies, and the high number of such objects in our sample, their typical SED should be well represented by the E/S0 template described above. In fact, although the IR signal of every single galaxy is lost in the stacking process, the E/S0 template still represents the average behavior of the early-type population of galaxies.

For every cluster we assign a  $r$ -band luminosity to all of its early-type members contained in the SDSS-maxBCG catalogue. For the BCG we use the value of  $L_r^{\text{BCG}}$ , while for the other galaxies we use the average luminosity of the non-BCG E/S0 galaxies, determined as

$$L_r^{\text{avg}} = \frac{L_r^{\text{memb}} - L_r^{\text{BCG}}}{N_{\text{gal}}^{R200} - 1}. \quad (4)$$

From eq. 3, we translated these  $r$ -band luminosities into IR luminosities:  $L_{\text{IR}} = R_{\text{IR},r} \times L_r$ , subsequently used to normalise the SED and further on to derive the fluxes in the  $60 \mu\text{m}$  and  $100 \mu\text{m}$  IRAS bands (see Sect. 5).

### 3.2. Contribution of late-type galaxies

Although the majority of optically bright galaxies in clusters environment are elliptical, and despite spiral galaxies in dense environments tend to be quickly stripped of their gas and have their star-formation quenched, they are still expected to provide a dominant contribution to the IR emission, due to their higher SFRs. Therefore, the contribution of late-type galaxies to the IR emission is crucial for our purposes and should be carefully estimated. Given the fact that late-type galaxies are not considered in the SDSS-maxBCG catalogue, their contribution was computed based on available modelings of galaxy populations, in particular the distribution of galaxies as a function of spectral type and luminosity. Since our sample goes from galaxy groups to rich clusters, we have included the environment dependence of these variables.

We based our model on the known properties of galaxies in the local universe as given by Balogh et al. (2004) who analysed the bimodal distribution of galaxies in a local ( $z < 0.08$ ) sample of SDSS galaxies (DR1). These authors performed a detailed study on the color and luminosity distribution of galaxies as a function of their environment for both early and late-type galaxies. For each galaxy they define a density estimator  $\Sigma_5$  which represents the local projected galaxy density ( $M_r < -20$ ) in  $\text{Mpc}^{-2}$  and they use it to classify the different environmental regimes. Beside  $N_{\text{gal}}^{R200}$  mentioned before (see Sect. 2.1), the SDSS-maxBCG dataset contains also information about the number of galaxies  $N_{\text{gal}}$  projected within a distance lower than  $1 h^{-1} \text{Mpc}$  from the BCG, with the magnitude limit of  $M_r < -16$ . Therefore for each cluster we can assume a unique value of  $\Sigma_5$  for all of its members by establishing a relation with  $N_{\text{gal}}$  and, finally, with the properties of the population of late-type galaxies present.

We proceed as follows.

- i) First of all, we integrate the double gaussian distributions of red and blue galaxies (Fig. 1 of Balogh et al. 2004) obtaining a ratio of red and blue galaxies for the 5 values of  $\Sigma_5$  considered: for our work, we only need the three density bins corresponding to dense environments (i.e. groups and clusters,  $\Sigma_5 > 0.5$ ). In these bins the resulting spiral fractions are  $f_{\text{spt}} = 0.597, 0.478$  and  $0.286$ , in order of increasing density.

- ii) In order to use these values for our calculations we need, at first, to correct the value of  $N_{\text{gal}}$ . The galaxy samples of Koester et al. (2007), in fact, has a magnitude limit  $M_r < -16$  while the definition of  $\Sigma_5$  includes only galaxies with  $M_r < -20$ : for this reason we use the red galaxies luminosity function (LF) given by Baldry et al. (2004) to calculate the number of expected galaxy members with  $M_r < -20$ . We obtained  $\langle N_{\text{gal}}^{-20} \rangle = 0.32 N_{\text{gal}}$ . As for Balogh et al. (2004), the sample of Baldry et al. (2004) is constituted by local SDSS galaxies, with the difference that it contains no density distinction (e.g. field galaxies). Therefore, by using the LF of Baldry et al. (2004) for this calculation we neglect the effect of environmental properties; anyway, since red galaxies are mostly present in galaxy clusters, we do not expect this to change significantly our results.
- iii) We are now able to obtain a first estimation of the density parameter associated to every cluster with the formula

$$\Sigma_{5,0} = \frac{\langle N_{\text{gal}}^{-20} \rangle}{1 - f_{\text{spi},0}} \frac{h^2}{\pi(1\text{Mpc})^2}, \quad (5)$$

where  $f_{\text{spi},0}$  is the fraction of spiral galaxy (with  $M_r < -20$ ) that for this calculation we fix arbitrarily to the initial value to  $f_{\text{spi},0} = 0.3$ .

- iv) Using the value of  $\Sigma_{5,0}$  we calculate a new estimate  $f_{\text{spi},1}$  of the spiral fraction by interpolating between the values of  $f_{\text{spi}}$  obtained by Balogh et al. (2004); this allows the calculation of a new value  $\Sigma_{5,1}$  of the galaxy density with equation 5.
- v) We repeat this procedure until  $\Sigma_{5,i}$  and  $f_{\text{spi},i}$  converge to definite values and check that the result does not depend on the initial choice of  $f_{\text{spi},0}$ , thus obtaining the expected number of spiral galaxies with  $M_r < -20$

$$\langle N_{\text{spi}}^{-20} \rangle = \langle N_{\text{gal}}^{-20} \rangle \times \frac{f_{\text{spi}}}{1 - f_{\text{spi}}} \times \frac{N_{\text{gal}}^{R200}}{N_{\text{gal}}}, \quad (6)$$

where the factor  $N_{\text{gal}}^{R200}/N_{\text{gal}}$  accounts for the ratio between the galaxies inside  $R_{200}$  and  $1h^{-1}$  Mpc.

- vi) Finally, we add the expected number of spiral galaxies in the magnitude range  $-20 < M_r < -18$  by referring again to the galaxy distributions of Balogh et al. (2004), thus obtaining for every cluster the estimated value of the number of spiral members with  $M_r < -18$ ,  $\langle N_{\text{spi}} \rangle$ . This value is then used as the average of a poissonian distribution, that we assumed to assign a randomised number of spiral  $N_{\text{spi}}$  to each cluster, thus to determine the total cluster galaxies:  $N_{200} = N_{\text{gal}}^{R200} + N_{\text{spi}}$ .

This formalism led us to derive an average fraction of about 30% spiral galaxies in our sample of SDSS-maxBCG clusters (see Table 1). The relation between  $N_{\text{gal}}$  and the fraction of spiral galaxies inside the whole cluster is shown in Fig. 2. When considering galaxies with the same magnitude limit (dashed line), the spiral fraction can be higher than 0.5 for groups and small clusters, and then lessens with increasing  $N_{\text{gal}}$  down to  $\sim 0.4$  for  $N_{\text{gal}}=70$ . When considering all the galaxies included in our model (i.e.  $M_r < -16$  for early-type and  $M_r < -18$  for late-type, solid line) the spiral fraction becomes lower by about 0.2.

The morphology-density study of Balogh et al. (2004) becomes useful also to assign a magnitude and a color to each spiral galaxy. For a given value of  $\Sigma_5$  it is possible to construct a probability distribution  $\mathcal{P}(M_r, u-r)$  for a late-type galaxy to have a given magnitude  $M_r$  and a given intrinsic color  $u-r$ . The

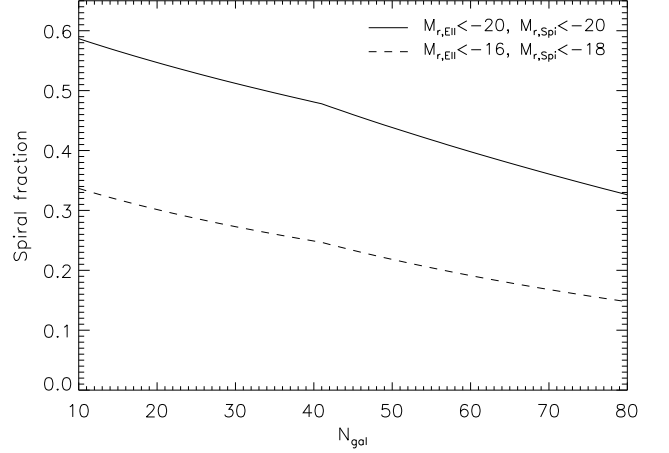


**Fig. 2.** Fraction of spiral galaxies within  $R_{200}$  (see Sect. 2.1 for the definition of  $R_{200}$ ) as a function of  $N_{\text{gal}}$ . The solid line represents the result obtained when considering only galaxies with  $M_r < -20$  (i.e. the magnitude limit used to calculate  $\Sigma_5$  in Balogh et al. 2004). The dashed line is the result obtained by considering all the galaxies included in our model: late-type galaxies with  $M_r < -18$  and early-type galaxies with  $M_r < -16$  from the SDSS-maxBCG catalogue. These functions have been calculated neglecting the evolution of the spiral fraction with redshift.

former value is used to determine the luminosity  $L_r$  in the  $r$ -band as

$$L_r = L_{0,r} 10^{-0.4M_r}, \quad (7)$$

where  $L_{0,r} = 2.15 \times 10^{34}$  erg/s is the luminosity of an object with  $M_r = 0$ , while the latter is used to assign the spectral type, according to the intervals shown in Table 1. To define these intervals we calculated the  $u-r$  colors of our GRASIL templates (2.40, 2.01 and 1.55 for the Sa, Sb and Sc, respectively) and defined the limits in order to associate to every galaxy the template that best approximates its value of  $u-r$ . We also checked the consistency of these numbers with the observed colors of local galaxies as reported by Fukugita et al. (1995) for the SDSS photometric system<sup>2</sup>. For what concerns starburst galaxies, the limit of  $u-r < 1.0$  has been taken directly from Fukugita et al. (1995) for irregular galaxies, since the  $u-r$  of our M82 templates ( $u-r = 2.10$ ) is not representative of the starburst galaxies population. However, we will show that the choice of this limit has a negligible impact on our final results. Finally, the luminosity  $L_{\text{IR}}$  is obtained from Eq. 3, where  $R_{\text{IR},r}$  is chosen according to the spectral type.

### 3.3. Evolution with redshift of spiral galaxies

Despite being the SDSS-maxBCG a catalogue of relatively nearby groups and clusters ( $0.1 < z < 0.3$ ), it is necessary to take into account the evolution with redshift of the late-type galaxies properties with respect to the results of Balogh et al. (2004) which are derived from a local (i.e.  $z < 0.08$ ) sample of SDSS galaxies. For the purpose of our modelisation we consider the sample of Balogh et al. (2004) as representative

<sup>2</sup> Referring to their Table 3, they obtain  $u-r$  colors of 2.26 for Sab and 1.68 for Sbc, thus close to our assumptions for the Sa/Sb and Sb/Sc limits, respectively.

of the galaxy population at  $z_B = 0.04$ , the central value of the interval, and apply two independent evolution effects.

### Spiral fraction evolution

It is generally accepted that in a hierarchical structure formation scenario spiral galaxies tend to evolve towards S0 or ellipticals. This can happen either passively, with the consumption of the gas reservoir and its ejection with SNe explosions, or it can also be triggered by environmental interactions with other galaxies and with the ICM (see Boselli & Gavazzi 2006a, for a review): it is therefore expected that the fraction of late-type galaxies increases with redshift (the so called Butcher-Oemler effect, Butcher & Oemler 1984). In fact, Laganá et al. (2009) find a change from about 0.1 to 0.3 in the spiral fraction of 20 galaxy clusters in the interval  $0 < z < 0.25$ . Fitting the data on the fraction of star-forming galaxies of these clusters, they quantify its redshift evolution as:  $\frac{df_{\text{spi}}}{dz} = 1.3 \pm 0.6$  (private communication). A similar result has been obtained by De Lucia et al. (2007), who find  $\frac{df_{\text{spi}}}{dz} \sim 1.1$  in the range  $0.4 < z < 0.8$ . Given the redshift interval of the SDSS-maxBCG catalogue, we take as a reference the value of Laganá et al. (2009). Despite this sample contains rather massive objects ( $k_B T$  from  $\sim 3$  to  $\sim 10$  keV), it should provide a first-order representation of the spiral fraction evolution in the redshift range of the SDSS-maxBCG catalogue. We therefore correct the number of spiral galaxies obtained in Section 3.2 with the following formula:

$$\langle N_{\text{spi}}(z) \rangle = [1 + 1.3(z - z_B)] \langle N_{\text{spi}} \rangle_{z=0} \quad (8)$$

Including this effect in our modelisation raises the global spiral fraction of our sample from 30% to 35%, as shown in Table 1. Although this number may seem high for clusters (see e.g. Bai et al. 2006, for the Coma cluster) we must consider that the SDSS-maxBCG catalogue is dominated by groups and small clusters, as mentioned in Section 2.1. However, when applying our model to the case of MS 1054-03 as observed by Bai et al. (2007) ( $z = 0.83$ ,  $N_{200} = 144$ ), we obtain  $f_{\text{spi}} = 0.16$  which is consistent within a  $1\sigma$  limit with the value of  $0.13 \pm 0.03$  found by the authors.

### Luminosity evolution

The current hierarchical structure formation scenario predicts that the peak of the star-formation is to be placed at  $z \approx 2 - 3$  and that at later epochs galaxies are mainly consuming their reservoir of gas. For this reason, when modeling the IR emission in the redshift range of the SDSS-maxBCG cluster sample we must consider that higher SFRs are expected with respect to the local galaxies. This effect has been widely observed and quantified. We take as a reference the evolution of the IR-luminosity observed by Le Floch et al. (2005): when parameterising it in the form of  $L_{\text{IR}} \propto (1+z)^{\alpha_L}$ , they obtain  $\alpha_L = 3.2^{+0.7}_{-0.2}$  over a sample of 2 635 objects identified at  $24 \mu\text{m}$  in the *Chandra* Deep Field South in the redshift range  $0 < z \lesssim 1$ . This result has been obtained by analysing field galaxies and this might introduce an environment bias on our results. Anyway, since it is expected that local star-forming galaxies inside clusters were the latest accreted, we can assume that this evolution scenario is valid also in cluster and group environments. Moreover, as shown in figure 3 of Giard et al. (2008), this assumption is backed-up by the *Spitzer* observation of the distant cluster MS1054-03 (Bai et al. 2007). Another bias may be introduced by the fact that these objects were identified directly in the mid-IR and not in the optical as for the galaxies of our sample. Therefore the galaxies of this sample are brighter than the ones of the

SDSS-maxBCG, both in the IR and in the optical. However, the total luminosity of the sample of Le Floch et al. (2005) is dominated by luminous ( $L_{\text{IR}} > 10^{11} L_{\odot}$ ) massive galaxies, which are the ones that provide most of the signal also in the IRAS bands. Therefore, we assume that their result can be applied also to the SDSS-maxBCG cluster sample to describe its global IR luminosity evolution. Consequently, we determine the IR luminosity  $L_{\text{IR}}$  as a function of redshift:

$$L_{\text{IR}}(z) = L_{\text{IR},0}(1+z-z_B)^{3.2}, \quad (9)$$

where  $L_{\text{IR},0}$  is the luminosity obtained by the magnitude  $M_r$  as from eq.7.

We do not include any specific effect of spiral population evolution towards bluer types with increasing redshift. In fact, the fraction of the different spectral types of spirals in the redshift range we are interested in is not expected to differ significantly with respect to the local galaxies inside galaxy clusters (see e.g. De Lucia et al. 2007). Moreover the consequent effect of slightly increased global luminosity is anyway partially included when assuming the luminosity evolution with redshift aforementioned.

### 3.4. Uncertainties on the model parameters

The choice of the values of the different parameters introduces a degree of uncertainty in our modelisation, the most important of which are connected with the choice of the redshift evolution parameters and the  $u-r$  color intervals used to define the spiral types (see Table 1). In order to quantify these uncertainties, we introduce two other sets of parameters to define a conservative and an extreme scenario and we will use the values of the fluxes estimated with these models to define the degree of confidence of our results. More precisely, for what concerns the redshift evolution we adopt the  $\pm 1\sigma$  values for  $\frac{df_{\text{spi}}}{dz} = (0.7, 1.9)$  and  $\alpha_L = (3.0, 3.9)$ , as measured by Laganá et al. (2009) and Le Floch et al. (2005), respectively. Moreover, we also artificially add a shift in the  $u-r$  color intervals of  $\pm 0.1$  in order to obtain a redder (conservative scenario) and a bluer (extreme) spiral population. Anyway, these changes introduce only minor modifications in the galaxy population: the difference in the global spiral fraction is of  $\sim 2\%$ , while the only significant change is in the fraction of starburst galaxies that goes from 0.2% in the conservative model to 1.1% in the extreme one. On the whole, the difference in the final fluxes is mainly introduced by the modified luminosity evolution. The results on the galaxy population for the conservative model are also shown in Table 1.

### 3.5. The IR luminosity function of the SDSS-maxBCG galaxies

We show in Fig. 3 the luminosity function of the galaxies included in our reference model, for the different spectral types. The luminosity considered is given in the rest-frame  $60 \mu\text{m}$  IRAS band.

The luminosities go from a minimum of  $\sim 10^8 L_{\odot}$  for the fainter E/S0 galaxies up to a maximum of some  $10^{11} L_{\odot}$  for the brightest spirals. Each type of spiral has a luminosity range of about 2 orders of magnitudes: this is a consequence of our method (see Sect. 3.2), that held the spiral magnitudes within the interval  $-23 < M_r < -18$  which corresponds to a factor of  $10^{0.4 \Delta M_r} = 100$  in luminosity with the only possible modification introduced by the redshift evolution. Anyway, we don't expect this limitation to affect significantly our results. In fact, this



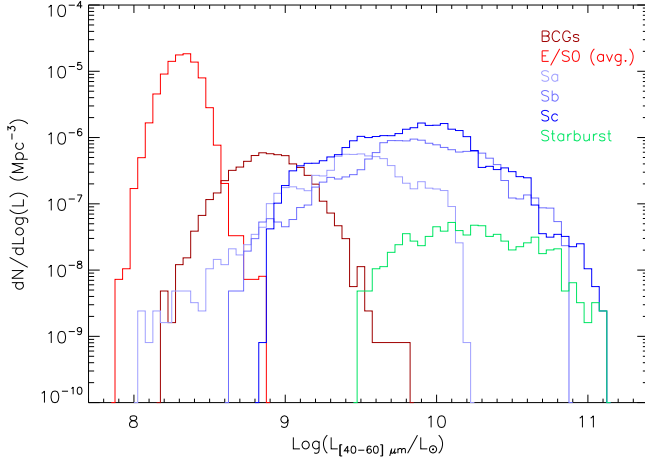


**Fig. 3.** Luminosity functions of each spectral type implemented in our model in the IRAS 60  $\mu\text{m}$  (i.e. top hat band-pass within [40,80]  $\mu\text{m}$ ). Spectral types are color-coded as follow: (i) early-type galaxies as (dark-red) for the BCGs and (light-red) for the other E/S0s (we assigned to every galaxy the average luminosity of the E/S0 members of each cluster, as shown in eq. 4); (ii) normal late-type galaxies, with Sa, Sb, Sc going from (light-blue) to (dark-blue), respectively; (iii) starburst galaxies as (green).

limit range is wider than the one covered by the distribution of the BCGs, which are the only galaxies for which we have direct observational constraints. On the contrary the E/S0 curve appears narrower because we considered the average luminosity of the E/S0 galaxies inside each cluster, thus limiting the dispersion of the E/S0 galaxies to the dispersion of the cluster luminosities.

When considering the luminosity function in the 100  $\mu\text{m}$  IRAS band the range and shape is similar for all the spectral types. Only starbursts are a factor  $\sim 3$  fainter in this band due to the drop in luminosity (see Fig. 1) which is due to an average higher galactic dust temperature compared to non-starburst.

## 4. Other galactic components

In this Section we try to put some constraints on the impact of three components of galactic origin which are not included in our modelisation of the IR emission of cluster galaxies: a missed population of faint galaxies, the possible presence of dust-embedded AGNs and the IR emission coming from heavily obscured star-forming galaxies. In all of these cases we conclude that their impact on our final results is probably very small, if not completely negligible.

### 4.1. Faint galaxy population

As mentioned in Sect. 3, our modelisation includes red galaxies with  $M_r < -16$  (the limit of the SDSS-maxBCG catalogue) and blue galaxies with  $M_r < -18$ , thus neglecting the signal of fainter objects, that may not be identified by the SDSS observations although present inside the cluster. We try to obtain a rough estimation of the impact of these objects on the total emission by referring to the luminosity functions obtained by Baldry et al. (2004) (see their Fig. 7).

For what concerns early-type galaxies, the faint-end of the LF ( $M^* = -21.49$ ,  $\alpha = -0.83$  in the Schechter function param-

eterisation) has a negative slope, so the number of galaxies is expected to diminish at higher magnitudes. For this reason no significant impact can be associated to these objects.

On the other side, the faint-end of the blue galaxies LF ( $M^* = -20.60$ ,  $\alpha = -1.35$ ) has a positive slope, so an increasing number of galaxies is expected with lower luminosities. For simplicity, we consider the assumption that all galaxies with  $M_r < -18$  have been included in our modelisation, then we integrate the late-type LF  $\phi_b(M_r)$  of Baldry et al. (2004) splitting it in two at this magnitude limit. We obtain

$$\frac{L_{\text{faint}}}{L_{\text{bright}}} = \frac{\int_{-18}^{\infty} \phi_b(M_r) L(M_r) dM}{\int_{-23}^{-18} \phi_b(M_r) L(M_r) dM} = 0.13, \quad (10)$$

where  $L(M_r)$  is the luminosity as a function of the magnitude  $M_r$ , thus indicating that the emission of the faint galaxy population is marginal with respect to the bright one.

Moreover, since the LF of Baldry et al. (2004) is obtained with the observation of field galaxies, it is reasonable to expect that in cluster environments the faint-end of the LF would be shallower, if not even negative, due to the processes of merging that affect particularly the smaller objects. Therefore the ratio of 0.13 obtained in eq. 10 can be safely considered an upper limit of the true value. For these reasons, and considering the assumption of the connection between the luminosity in the optical and IR bands used throughout this work, we can conclude that even if we can not exclude the presence of the signal of a population of faint ( $M_r > -18$ ) unresolved galaxies, we expect that the contribution of faint star-forming galaxies to be marginal.

### 4.2. Dusty AGNs

When estimating the total IR luminosities of the galaxies of our sample, we do not take into account what could be the contribution of AGN deeply embedded in dusty cocoons within cluster galaxies.

In fact, recent results indicate the existence of a population of heavily absorbed AGNs in the field (see e.g. Fiore et al. 2009; Lanzuisi et al. 2009): these objects are detectable at IR wavelengths. Although optical observations indicate a very small fraction of cluster galaxies with detected AGNs ( $\sim 1\%$ , see e.g. Dressler et al. 1999), some X-ray observations have detected an excess of point sources associated to AGNs in cluster fields. For example, Martini et al. (2006) observed with *Chandra* a sample of 8 low redshift ( $z \lesssim 0.3$ ) clusters, finding  $\sim 5\%$  of their galaxy members hosting an AGN, most of which are not detected with optical surveys. These AGNs are also present in E/S0 galaxies, and whilst they are obscured in the optical (their emission being heavily absorbed), they could be bright in the IR. Therefore, they could contribute to the total IR cluster emission.

It is difficult to quantify with precision the impact on the total IR signal of these kinds of objects. We take as a reference the work done by Bai et al. (2007), who studied the IR properties of the galaxies of MS1054-03 ( $z = 0.83$ ) with the *Spitzer* satellite. They identified eight point sources with X-ray and radio observations that could be associated with AGNs: anyway, only three of these objects have an IR counterpart over the 144 IR-detected cluster members, and only one of these is associated with a bright star-forming object. For these reasons the authors conclude that the contamination from AGNs is negligible. Similar conclusions have been drawn by Bai et al. (2006) in their study of the Coma cluster ( $z = 0.023$ ).

Even if they are based on single cluster studies, these results, which have been obtained both at redshift higher and lower than

our cluster sample, indicate that the impact of AGN contamination in the observations of Giard et al. (2008) is probably very small.

#### 4.3. Heavily obscured star-forming galaxies

Optical observations have highlighted the fact that some galaxy clusters host heavily obscured star-forming galaxies. In the framework of our modelisation, the presence of these objects would lead to an underestimate of their IR emission based on the optical one (see Metcalfe et al. 2005, for a review). In particular, IR observations on A1689 (Duc et al. 2002), J1888.16CL (Duc et al. 2004), CL0024+1654 (Coia et al. 2005) and, more recently, on A1758 (Haines et al. 2009) have revealed galaxies with much higher SFRs with respect to what is expected from optical diagnostics (e.g. [OII]). However, all of these clusters show clear signs of recent dynamical activities, like major mergers and significant accretion of galaxies from the field, thus suggesting that these phenomena are responsible of the star-formation triggering. Since our cluster sample is at a relatively low redshift, we do not expect it to contain a high fraction of dynamically active haloes and, therefore, to be significantly affected by the presence of heavily obscured star-formation.

### 5. Reconstructing the stacked IR flux

As mentioned before the main objective of this work is to explain the origin of the IR emission observed in the direction of galaxy clusters by Montier & Giard (2005) and Giard et al. (2008). Therefore, we want to compare the flux expected out of our model from the galactic emission in the 60  $\mu\text{m}$  and 100  $\mu\text{m}$  IRAS bands with the one measured by Giard et al. (2008). In order to do so, we need to compute for every single cluster the expected flux taking into account the instrumental beam and the spectral band pass of the IRAS satellite.

We assume that every galaxy is placed at the redshift  $z$  of the cluster to which it belongs and we compute its flux  $F_{\lambda_0}^3$  in a given band

$$F_{\lambda_0} = \frac{1}{4\pi d_L^2 \Delta\nu_0} \int L\left(\frac{\lambda}{1+z}\right) f_{\lambda_0}(\lambda) d\lambda, \quad (11)$$

where  $\Delta\nu_0$  is the frequency interval of the corresponding band,

$$d_L(z) = \frac{c(1+z)}{H_0} \int_0^z \frac{dz'}{\sqrt{\Omega_m(1+z')^3 + \Omega_\Lambda}} \quad (12)$$

is the luminosity distance of the cluster ( $H_0 \equiv 100h \text{ km s}^{-1} \text{ Mpc}^{-1}$ ),  $f_{\lambda_0}(\lambda)$  is the IRAS spectral response function in a given band (i.e.  $\lambda_0 = 60, 100 \mu\text{m}$ ) which is convolved<sup>4</sup> with the SED  $L(\lambda)$  of the spectral type of each cluster galaxy, normalised according to the value of  $L_{\text{IR}}$  (see Sect. 3).

The stacked signals by Giard et al. (2008) are integrated fluxes over an angular area of  $10'$  of radius centered on the cluster (see Sect. 2 for details). Since the IRAS FWHM beams are  $4'$  and  $4.5'$  at 60 and 100  $\mu\text{m}$  respectively, thus comparable to the size of the observed field, we need to take into account the

possible loss of signal from galaxies distant from the cluster center due to the convolution with the instrumental beam. In order to model this effect, we have to distribute the cluster galaxies in the cluster potential well. We thus randomly assign to every galaxy a distance from the BCG (considered to be at the cluster center, thus at the center of the  $10'$  field) by assuming that their spatial distribution follows a NFW profile (Navarro et al. 1997). The two parameters needed to characterise the NFW profile are  $R_{200}$  and the concentration  $c$ . They were obtained from the richness  $N_{\text{gal}}^{R200}$  of each halo (see Sect. 2.1) and by adopting the  $N - M$  scaling relation of Rykoff et al. (2008) derived from the SDSS-maxBCG, and the  $(M, z) - c$  relation of Dolag et al. (2004) derived from numerical simulations. Then for every galaxy we compute the fraction of the signal that falls inside the observed region in the two bands. This effect proves to be completely negligible as globally less than one per cent of the signal falls outside the field in both bands. Since galaxies of later spectral types are expected to be more spread than ellipticals, as a result of their recent accretion into the cluster (see, e.g., the discussion in Popesso et al. 2005), we repeated our estimation on the possible lost signal by assuming that late-type galaxies are distributed uniformly in a sphere of radius  $R_{200}$ : even with this extreme hypothesis the amount of signal that is expected to fall outside the field remains negligible (about 3% of the total). The low impact of this effect on the global results can also be seen from the distributions of the angular sizes of  $R_{200}$  obtained with this method shown in Fig. 4 for different redshift bins. More than 70% of the clusters have angular sizes lower than  $5'$  and only in the lowest redshift bin some objects (43) exceed the  $10'$  aperture.

With the stacking technique adopted by Giard et al. (2008), it is clear that also the signal coming from foreground/background objects is present in the observed fields. Anyway, as said in Section 2, the authors adopted a background subtraction based on the signal in the fields adjacent to every map, relying on the high statistical robustness of their sample. For this reason we can safely conclude that the emission of foreground/background objects has been successfully subtracted, thus we do not need to include it in our modelisation.

### 6. Results and discussion

#### 6.1. Predicted and observed IR fluxes

Our estimations of the 60 and 100  $\mu\text{m}$  fluxes from cluster galaxies are reported in Table 2, associated to the emission calculated with our model for the different galaxy populations.

The total flux due to the early-type galaxies estimated with our model is 39.3 Jy at 60  $\mu\text{m}$  band and 79.4 Jy in the 100  $\mu\text{m}$  band, accounting for about 7% of and 6%, respectively, of the fluxes measured in the same bands by Giard et al. (2008). In both bands about 20% of the E/S0 signal comes from the BCGs.

As expected, late-type galaxies constitute by far the most significant contribution to the IR emission. According to our reference model they contribute to 645.2 Jy at 60  $\mu\text{m}$  and 1904.8 Jy at 100  $\mu\text{m}$  thus accounting for about 95% of the total galactic emission. This contribution comes mostly from the Sb and Sc population, with the Sc being widely dominant in the 100  $\mu\text{m}$  band.

Despite their high luminosities, we predict that starburst galaxies do not provide a significant contribution to the IR emission, due to their low expected number. We obtain a contribution of 15.4 Jy at 60  $\mu\text{m}$  and 12.1 Jy at 100  $\mu\text{m}$  corresponding respectively to about 2% and 0.5% of total predicted signal. Only in our extreme scenario their contribution becomes non-negligible

<sup>3</sup> This quantity corresponds to a flux per unit frequency (e.g. Jy). Anyway we prefer to use the notation  $F_\lambda$ , rather than  $F_\nu$ , to refer directly to the fluxes  $F_{60}$  and  $F_{100}$  in the 60 and 100  $\mu\text{m}$  bands, respectively.

<sup>4</sup> For these calculations we used the tools of the DUSTEM code, an updated version of the emission model of Desert et al. (1990), which contains details on the IRAS response functions in the different bands.



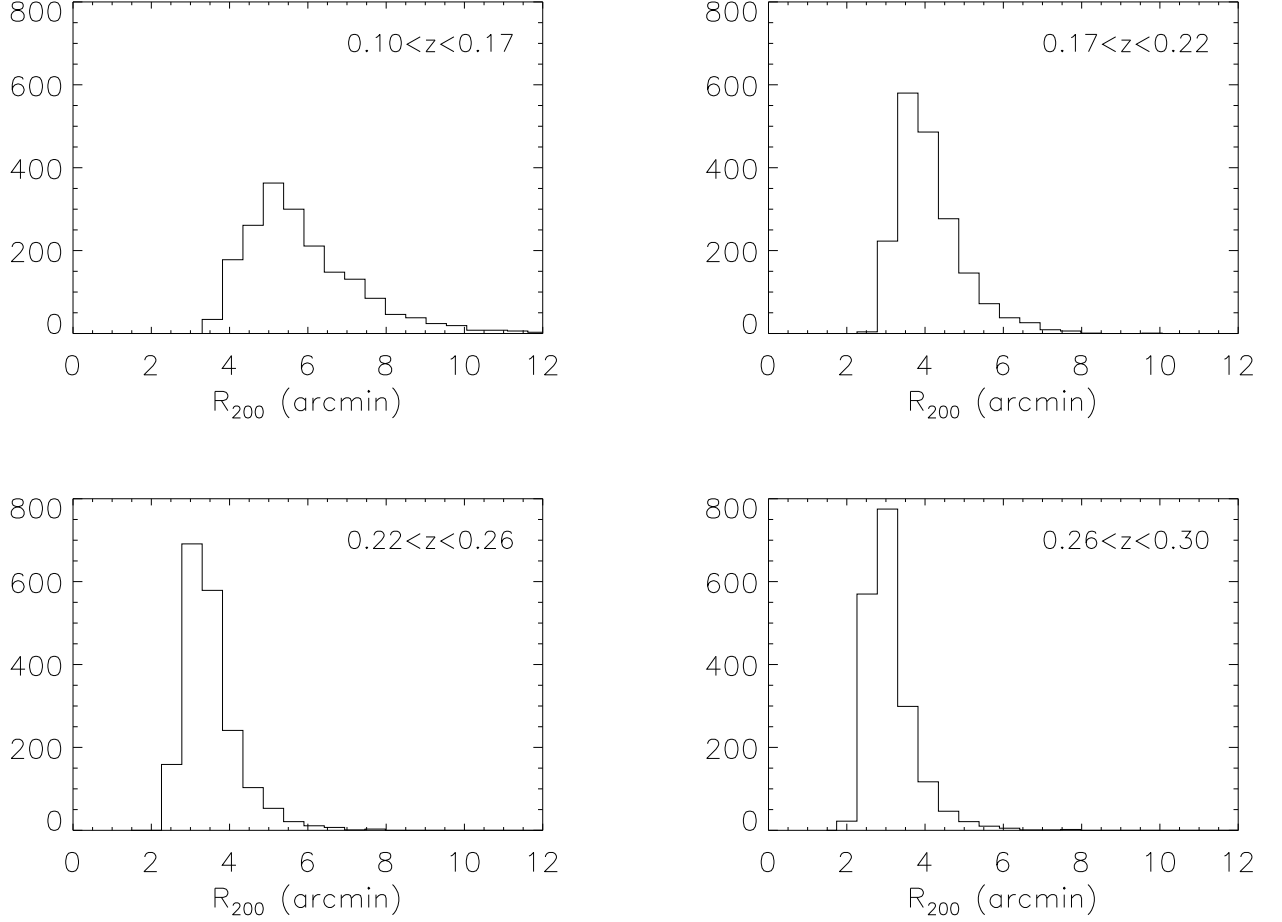


**Fig. 4.** Distribution of the angular sizes of  $R_{200}$  for the cluster sample in 4 redshift intervals chosen in order to contain the same number of clusters (i.e. 1869). The bin size of each histogram is 0.5 arcmin.

**Table 2.** Estimated fluxes in the 60  $\mu\text{m}$  and 100  $\mu\text{m}$  IRAS bands from the galaxy population of the SDSS-maxBCG clusters.

Spectral type	$F_{60}$ (Jy)	$F_{100}$ (Jy)
<i>-Early-type</i>		
BCG	8.2	16.5
E/S0	31.1	62.9
(Total early-type)	(39.3)	(79.4)
<i>-Late-type</i>		
Sa	36.4	58.6
Sb	259.5	621.3
Sc	333.9	1133.4
Starburst	15.4	12.1
(Total late-type)	(645.2)	(1825.4)
Total	$684.5^{+211.3}_{-138.0}$	$1904.8^{+617.1}_{-429.1}$
Observed	$570.1 \pm 36.1$	$1359.9 \pm 249.1$

We show the total fluxes and contribution of each galaxy population included in our model. The quoted errors on the total values correspond to the differences between our reference model and the conservative and extreme scenarios described in Section 3.4. The measurements by Giard et al. (2008) are reported together with their  $1\sigma$  error bars.

in the 60  $\mu\text{m}$  band, reaching the 5% of the total predicted flux. This low contribution agrees with the low rate of starburst galaxies as found in the field by Le Floch et al. (2005) at the redshift range of the SDSS-maxBCG catalogue (i.e.  $0.1 < z < 0.3$ ).

The total fluxes associated to the galactic emission predicted by our reference model are 684.5 [546.5, 895.8] Jy at 60  $\mu\text{m}$  and 1904.8 [1475.7, 2521.9] Jy at 100  $\mu\text{m}$  (the bracketed interval indicate the values derived from our conservative and extreme models, see Sect. 3.4). It appears that the reconstructed IR emission due to the galactic dust emission of the cluster members can explain the entire signal measured by Giard et al. (2008), with an indication that our reference model overestimates the total flux, particularly at 100  $\mu\text{m}$ . Indeed, these authors obtained  $570.1 \pm 36.1$  Jy and  $1359.9 \pm 249.1$  Jy at 60  $\mu\text{m}$  and 100  $\mu\text{m}$ , respectively. We will propose an explanation of this discrepancy in the next sections. However, when considering our conservative scenario, the predicted emission is in good agreement with the total measured signal in both bands.

Given these results, modulo the uncertainties of our modelisation, we obtain that the IR emission of the galaxy members is consistent with the total observed emission of our clusters sample, leaving little space to the possible presence of other components like intracluster dust.

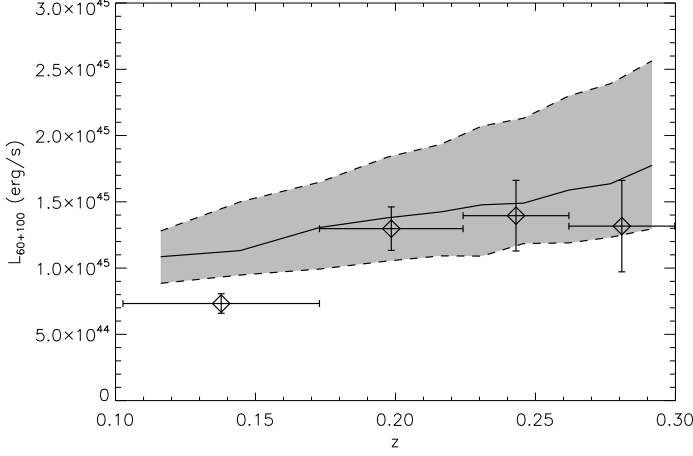


**Fig. 5.** Average cluster luminosities (see eq. 13) as a function of redshift. Diamonds represent the measurements and associated  $1\sigma$  error bars by Giard et al. (2008) in 4 redshift bins, defined in order to contain the same number of clusters (i.e. 1869). The solid line represents the average luminosity of the clusters in our reference model. The two dashed lines show the corresponding luminosity of the conservative and extreme model (see Section 3.4 for the details).

### 6.2. Redshift evolution

In this Section we characterise the redshift evolution of the average clusters luminosity. Following Desert et al. (1990), we define the total luminosity in the 60 and 100  $\mu\text{m}$  IRAS bands as

$$L_{60+100} \equiv 4\pi d_L^2 \times \left[ \lambda \frac{\Delta\nu}{\Delta\lambda} F_\lambda(60\mu\text{m}) + \lambda \frac{\Delta\nu}{\Delta\lambda} F_\lambda(100\mu\text{m}) \right], \quad (13)$$

where  $\Delta\nu$  and  $\Delta\lambda$  are the bandwidths in frequency and wavelength, respectively, of the two IRAS bands. This formula represents a good approximation of the total luminosity of our haloes at  $\lambda \gtrsim 40\mu\text{m}$ .

We show in Fig. 5 the average luminosity as obtained from eq. 13 for the clusters at different redshifts, both as predicted by our model and as observed by Giard et al. (2008). Our 4 bins are defined in order to contain the same number of clusters (i.e. 1869). This analysis shows clearly that the discrepancy between our reference model with respect to the observed fluxes is due to the low-redshift clusters only, which are responsible for most of the predicted flux. In fact, while our reference model is compatible within  $1\sigma$  with the results of Giard et al. (2008) in the 3 high-redshift bins, in the first bin ( $0.10 < z < 0.17$ ) the predicted luminosity is higher at  $6\sigma$  confidence. Our conservative scenario is also compatible with observed luminosities at  $z > 0.17$ , while the discrepancy for the low-redshift clusters persists at more than  $3\sigma$ . On the contrary, our extreme model is excluded by the results of Giard et al. (2008) through all the redshift range.

### 6.3. Selection bias

Our results indicate that although our model well describes the global IR emission of the SDSS-maxBCG galaxy clusters at  $z \gtrsim 0.17$ , the predicted galactic emission at low redshift clearly exceeds the measured stacked signal. The strong decrease in the IR luminosity is present also in the NED and NSC clusters samples analysed by Giard et al. (2008) and, as discussed in their

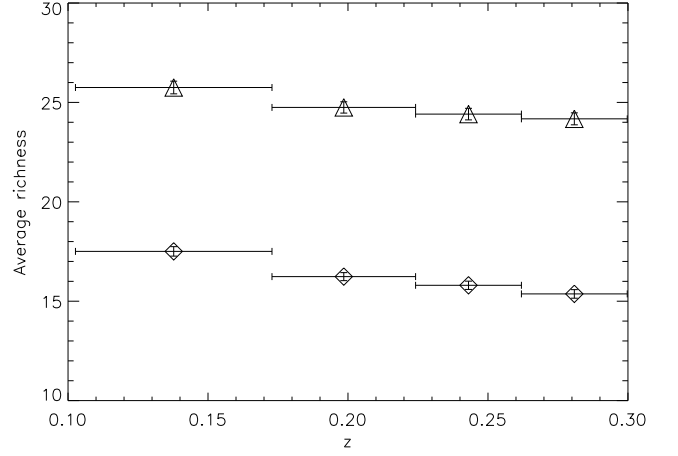


**Fig. 6.** Average richness as a function of redshift. Diamonds represent the average values of  $N_{\text{gal}}^{R200}$  (i.e. the number of E/S0 members) with associated  $1\sigma$  errorbars in 4 redshift bins defined as in Fig. 4 and 5. Triangles represent the values of  $N_{200}$  (i.e. total cluster members, see the definition in Section 3.2).

work, it can be interpreted as a selection effect which biases towards rich and massive clusters at high redshift as it is evident for the NSC sample (see their Fig. 6). However, this is not the case for the clusters object of our analysis. In Fig. 6 we show the average cluster richness in the same redshift bins both for the values of  $N_{\text{gal}}^{R200}$ , directly obtained from the SDSS-maxBCG catalogue, and  $N_{200}$  which includes late-type galaxies, as described in Section 3.2. It is clear that no selection bias is present in our clusters sample: on the contrary low-redshift clusters show slightly higher values of  $N_{\text{gal}}^{R200}$ . Even when including late-type galaxies this trend does not change significantly.

### 6.4. Effect of the cluster environment

These considerations indicate that the discrepancy between our model and the decrease of luminosity towards lower redshift must be connected with an evolution of the galaxy IR luminosity driven by the cluster environment, associated to gas and/or dust removal and consequent star-formation quenching. This can happen via ram-pressure stripping and tidal interaction. This picture is in agreement with the low number of high IR-to-optical galaxies observed in local galaxy clusters (see, e.g., Bica & Giovanelli 1987). A similar phenomenon is also seen in the observed properties of the galaxies of the Virgo cluster. In fact, Boselli et al. (2006) observed a truncation in the disk of NGC 4569 both in the UV and in the IR ( $8\text{--}70\mu\text{m}$ ) that they associate to a ram-pressure stripping of the external regions. More in general, Gavazzi et al. (2006) observe a consistent  $H_\alpha$  deficiency in Virgo galaxies which indicates a low SFR and diminished dust heating/emission (see also the discussion in Boselli & Gavazzi 2006a). In this scenario, once the star-formation quenching happens, the SEDs of the galaxy members would be consistently modified at the IR and UV wavelengths, being not compatible anymore with field galaxies, thus explaining the excess predicted by our model. However, we must point out that the environmental effects on the Virgo cluster are likely to be much stronger than what is expected for the population of clusters considered in our analysis. In fact, the Virgo cluster is about one order of magnitude more massive than the ma-

jority of the SDSS-maxBCG galaxy clusters and it shows several evidences of recent dynamical activity. On the contrary, being the SDSS-maxBCG cluster sample mainly constituted by small haloes (see Section 2.1), in the context of the hierarchical structure formation scenario it is reasonable to expect that they correspond to relaxed and dynamically old systems (see, for instance, the results on the concentration-mass relation of Dolag et al. 2004; Buote et al. 2007).

### 6.5. Constraints on intracluster dust

If we take as a reference our conservative scenario and compare its results with the average observed luminosity in the three high-redshift bins, we can estimate an upper limit on the possible emission due to extragalactic dust of about 10% of the total luminosity, which translates into a dust-to-gas mass abundance of  $Z_d \lesssim 5 \times 10^{-5}$  (see the discussion in Giard et al. 2008). This figure is in agreement with the expectations from theoretical models (Popescu et al. 2000; Aguirre et al. 2001) and with current observational upper limits on the dust abundance. Chelouche et al. (2007) analysed the reddening of a sample of quasars in the direction of the clusters of the SDSS-maxBCG catalogue, obtaining an estimate of  $Z_d \approx 10^{-5}$ . A similar result has also been obtained by Bovy et al. (2008) by measuring the dust absorption on the spectra of galaxies located behind local ( $z \sim 0.05$ ) galaxy clusters.

If on one side we do not see an evidence of intracluster dust emission in our sample, these last considerations leave an open question of how much dust has been lost by cluster galaxies polluting the ICM and if it can live enough to produce a significant diffuse IR emission. According to Popescu et al. (2000), the dust stripped from infalling galaxies will probably remain localised close to their parent galaxies without diffusing efficiently into the ICM. In any case, the strong decrease in the total cluster luminosity observed by Giard et al. (2008) compared to our results, suggests that, if present, the signal of intracluster dust should be very small.

## 7. Summary and conclusions

In this work we performed, for the first time, a thorough modelisation of the overall IR emission of galaxy clusters due to cluster galaxies IR emission. We tested the results of our model against the statistical stacking measurements of clusters IR emission in the 60 and 100  $\mu\text{m}$  IRAS bands by Giard et al. (2008), making use of the SDSS-maxBCG catalogue of groups and clusters (Koester et al. 2007).

We used the available SDSS-maxBCG data on the luminosity in the  $r$ -band of the cluster early-type members, and converted them into IR luminosities by adopting the model templates of the GRASIL code (Silva et al. 1998). Since the SDSS-maxBCG catalogue does not contain information on the late-type galaxies component, we used the results on the morphology-density relation obtained by Balogh et al. (2004) on a local SDSS galaxy sample to construct a model to statistically associate to every cluster its spiral galaxy population, namely the number of spiral members, their spectral type and their  $M_r$ . Again, this information on the optical properties has been used to obtain the corresponding IR emission by making use of 4 other GRASIL templates to represent normal late-type (Sa, Sb and Sc) and starburst galaxies. We also included in our model the expected redshift evolution of the spiral fraction and the IR luminosity by using results on observed galaxies in order to account for the possible difference in the spiral galaxy population of the

SDSS-maxBCG catalogue ( $0.1 < z < 0.3$ ) and the more local objects of the Balogh et al. (2004) sample ( $z < 0.08$ ).

Finally, we used our predictions to calculate the total expected galactic flux, by considering also the possible loss of signal due to the IRAS beam smoothing and the IRAS response function, and compared it with the measurements of Giard et al. (2008).

Our main results can be summarized as follows.

- i) According to our model, late-type galaxies represent about  $\sim 35\%$  of the galaxy population in nearby groups and clusters (i.e.  $z < 0.3$ ). This figure is coherent with the fact that this sample is dominated by groups and small clusters ( $N_{\text{gal}}^{R200} = 10 - 20$ ), thus letting this fraction of late-types falling between the field ( $f_{\text{spl}} \approx 0.5$ ) and the rich cluster ( $f_{\text{spl}} \approx 0.15$ ) regime.
- ii) As expected, normal late-type galaxies constitute the most important contribution to the total IR luminosity at 60 and 100  $\mu\text{m}$  accounting for  $\sim 95\%$  of the total galactic emission. Oppositely, the impact of starburst galaxies is marginal.
- iii) Early-type galaxies dominate the faint end of the LF in the IR and they account for the remaining  $\sim 5\%$  of the galactic contribution of the cluster IR emission.
- iv) Our model shows that the total flux estimated from the galaxy accounts, within uncertainties, for the entire stacked signal measured by Giard et al. (2008). With our reference model we obtain 684.5 Jy at 60  $\mu\text{m}$  and 1904.8 Jy at 100  $\mu\text{m}$ , which exceeds the stacked fluxes measured by Giard et al. (2008). However, when considering the uncertainties in our parameters, we showed that in a conservative scenario this discrepancy disappears.
- v) We compared the redshift distribution of the IR emission predicted by our model to the measurements of Giard et al. (2008) and found that the excess flux is present only in the clusters at lower redshift ( $z \lesssim 0.17$ ).

The results presented here show that the IR emission of galaxy clusters can be explained with its galactic component only, leaving very little room to the possible presence of any diffuse emission associated to intracluster dust. In this framework, the upper limit on the dust-to-gas mass abundance obtained by Giard et al. (2008) can be reduced by an order of magnitude, down to  $Z_d \lesssim 5 \times 10^{-5}$ . This result is in agreement with current estimations on the dust abundance in the ICM obtained from extinction and reddening measurements in the direction of SDSS clusters (Chelouche et al. 2007; Bovy et al. 2008).

The lack of diffuse dust, however, does not mean that the environment is not influencing the IR properties of its galaxy members. The fact that the predicted excess emission is concentrated in the lowest redshift objects indicates that the IR emission of late-type galaxies in local clusters is not completely compatible with their field equivalents. This result is in agreement with the lack of bright IR galaxies observed in several local clusters (see Boselli & Gavazzi 2006a, and references therein) and it is likely connected to the quenching of the star-forming activity driven by the cluster environment on its galaxy members, due to gas or dust removal: in this last case, the dust injected in the ICM is probably quickly depleted via sputtering processes. However, it is not clear why this could act significantly only at  $z \lesssim 0.2$  when most of the large-scale structures are already formed. For this reason, and given the limited redshift range of the SDSS-maxBCG catalogue, it would be interesting to extend our analysis to higher redshifts, where the SFR is expected to be higher and more dynamical activity is

expected at cluster scales.

*Acknowledgements.* We thank an anonymous referee who helped improving the presentation of our results. We are grateful to L. Silva for publishing some GRASIL templates in her webpage. We thank M. Balogh and T. F. Laganá for providing some additional data not published in their papers. We acknowledge useful discussions with S. Bardelli, J.-P. Bernard, A. Boselli, J. Lanoux, L. Pozzetti, F. Pozzi and C. Tonini. We are particularly grateful to A. Bongiorno for the help provided in the treatment of optical data. The authors L. Montier, E. Pointecouteau and M. Roncarelli acknowledge the support of grant ANR-06-JCJC-0141.

## References

- Abell, G. O., Corwin, Jr., H. G., & Olowin, R. P. 1989, *ApJS*, 70, 1
- Aguirre, A., Hernquist, L., Schaye, J., et al. 2001, *ApJ*, 561, 521
- Aguirre, A. & Schaye, J. 2007, in *EAS Publications Series*, Vol. 24, EAS Publications Series, ed. E. Emsellem, H. Wozniak, G. Massacrier, J.-F. Gonzalez, J. Devriendt, & N. Champavert, 165–175
- Arnaboldi, M. 2004, in *Baryons in Dark Matter Halos*, ed. R. Dettmar, U. Klein, & P. Salucci
- Arnaud, M. 2005, in *Background Microwave Radiation and Intracluster Cosmology*, ed. F. Melchiorri & Y. Rephaeli, 77–+
- Bai, L., Rieke, G. H., & Rieke, M. J. 2007, *ApJ*, 668, L5
- Bai, L., Rieke, G. H., Rieke, M. J., et al. 2006, *ApJ*, 639, 827
- Baldry, I. K., Glazebrook, K., Brinkmann, J., et al. 2004, *ApJ*, 600, 681
- Balogh, M. L., Baldry, I. K., Nichol, R., et al. 2004, *ApJ*, 615, L101
- Bicay, M. D. & Giovanelli, R. 1987, *ApJ*, 321, 645
- Biviano, A. 2008, *ArXiv e-prints*
- Blanton, M. R. & Roweis, S. 2007, *AJ*, 133, 734
- Borgani, S. 2008a, in *Lecture Notes in Physics*, Berlin Springer Verlag, Vol. 740, *A Pan-Chromatic View of Clusters of Galaxies and the Large-Scale Structure*, ed. M. Plionis, O. López-Cruz, & D. Hughes, 287–+
- Boselli, A., Boissier, S., Cortese, L., et al. 2006, *ApJ*, 651, 811
- Boselli, A. & Gavazzi, G. 2006a, *PASP*, 118, 517
- Bovy, J., Hogg, D. W., & Moustakas, J. 2008, *ApJ*, 688, 198
- Bower, R. G., Lucey, J. R., & Ellis, R. S. 1992, *MNRAS*, 254, 601
- Buote, D. A., Gastaldello, F., Humphrey, P. J., et al. 2007, *ApJ*, 664, 123
- Butcher, H. & Oemler, Jr., A. 1984, *ApJ*, 285, 426
- Chelouche, D., Koester, B. P., & Bowen, D. V. 2007, *ApJ*, 671, L97
- Coia, D., McBreen, B., Metcalfe, L., et al. 2005, *A&A*, 431, 433
- Conroy, C., Wechsler, R. H., & Kravtsov, A. V. 2007, *ApJ*, 668, 826
- da Silva, A. C., Catalano, A., Montier, L., et al. 2009, *MNRAS*, 396, 849
- De Lucia, G. et al. 2007, *MNRAS*, 374, 809
- Desert, F.-X., Boulanger, F., & Puget, J. L. 1990, *A&A*, 237, 215
- Dolag, K., Bartelmann, M., Perrotta, F., et al. 2004, *A&A*, 416, 853
- Dolag, K., Murante, G., & Borgani, S. 2009, *ArXiv e-prints*
- Dressler, A. 1980, *ApJ*, 236, 351
- Dressler, A., Oemler, A. J., Couch, W. J., et al. 1997, *ApJ*, 490, 577
- Dressler, A., Smail, I., Poggianti, B. M., et al. 1999, *ApJS*, 122, 51
- Duc, P.-A., Fadda, D., Poggianti, B., et al. 2004, 347
- Duc, P.-A., Poggianti, B. M., Fadda, D., et al. 2002, *A&A*, 382, 60
- Fabian, A. C., Sanders, J. S., Taylor, G. B., et al. 2006, *MNRAS*, 366, 417
- Fang, W. & Haiman, Z. 2008, *ApJ*, 680, 200
- Fiore, F. et al. 2009, *ApJ*, 693, 447
- Fukugita, M., Shimasaku, K., & Ichikawa, T. 1995, *PASP*, 107, 945
- Gal, R. R., de Carvalho, R. R., Lopes, P. A. A., et al. 2003, *AJ*, 125, 2064
- Gavazzi, G., Boselli, A., Cortese, L., et al. 2006, *A&A*, 446, 839
- Giard, M., Montier, L., Pointecouteau, E., & Simmat, E. 2008, *A&A*, 490, 547
- Haines, C. P., Smith, G. P., Egami, E., et al. 2009, *MNRAS*, 396, 1297
- Hansen, S. M., McKay, T. A., Wechsler, R. H., et al. 2005, *ApJ*, 633, 122
- Kapferer, W., Ferrari, C., Domainko, W., et al. 2006, *A&A*, 447, 827
- Koester, B. P. et al. 2007, *ApJ*, 660, 239
- Krick, J. E. & Bernstein, R. A. 2007, *AJ*, 134, 466
- Lagache, G., Puget, J.-L., & Dole, H. 2005, *ARA&A*, 43, 727
- Laganá, T. F., Dupke, R. A., Sodr , Jr., L., Lima Neto, G. B., & Durret, F. 2009, *MNRAS*, 394, 357
- Lanzuisi, G., Piconcelli, E., Fiore, F., et al. 2009, *A&A*, 498, 67
- Le Floch, E. et al. 2005, *ApJ*, 632, 169
- Mantz, A., Allen, S. W., Ebeling, H., & Rapetti, D. 2008, *MNRAS*, 387, 1179
- Mantz, A., Allen, S. W., Rapetti, D., & Ebeling, H. 2009, *ArXiv e-prints*
- Martini, P., Kelson, D. D., Kim, E., Mulchaey, J. S., & Athey, A. A. 2006, *ApJ*, 644, 116
- Mathis, J. S., Ruml, W., & Nordsieck, K. H. 1977, *ApJ*, 217, 425
- McNamara, B. R. & Nulsen, P. E. J. 2007, *ARA&A*, 45, 117
- Metcalfe, L., Fadda, D., & Biviano, A. 2005, *Space Science Reviews*, 119, 425
- Montier, L. A. & Giard, M. 2004, *A&A*, 417, 401
- Montier, L. A. & Giard, M. 2005, *A&A*, 439, 35
- Murante, G., Giovalli, M., Gerhard, O., et al. 2007, *MNRAS*, 377, 2
- Navarro, J. F., Frenk, C. S., & White, S. D. M. 1997, *ApJ*, 490, 493
- O’Dea, C. P., Baum, S. A., Privon, G., et al. 2008, *ApJ*, 681, 1035
- Pipino, A., Kaviraj, S., Bildfell, C., et al. 2009, *MNRAS*, 395, 462
- Popescu, C. C., Tuffs, R. J., Fischera, J., & V lk, H. 2000, *A&A*, 354, 480
- Popesso, P., Biviano, A., B hringer, H., Romaniello, M., & Voges, W. 2005, *A&A*, 433, 431
- Rykoff, E. S., McKay, T. A., Becker, M. R., et al. 2008, *ApJ*, 675, 1106
- Sarazin, C. L. 1988, *X-ray emission from clusters of galaxies* (Cambridge Astrophysics Series, Cambridge: Cambridge University Press, 1988)
- Schindler, S. & Diaferio, A. 2008, *Space Science Reviews*, 134, 363
- Sijacki, D. & Springel, V. 2006, *MNRAS*, 366, 397
- Silva, L., Granato, G. L., Bressan, A., & Danese, L. 1998, *ApJ*, 509, 103
- Soifer, B. T., Helou, G., & Werner, M. 2008, *ARA&A*, 46, 201
- Stickel, M., Klaas, U., Lemke, D., & Mattila, K. 2002, *A&A*, 383, 367
- Stickel, M., Lemke, D., Mattila, K., Haikala, L. K., & Haas, M. 1998, *A&A*, 329, 55
- Vikhlinin, A., Kravtsov, A. V., Burenin, R. A., et al. 2009, *ApJ*, 692, 1060
- Voges, W. 1992, *The ROSAT all-sky X ray survey*, Tech. rep.
- Voit, G. M. 2005, *Reviews of Modern Physics*, 77, 207
- Werner, N., Durret, F., Ohashi, T., Schindler, S., & Wiersma, R. P. C. 2008, *Space Science Reviews*, 134, 337